5. Cross-Phase Alignment of Segmented Nanorods

5.1. Introduction

In this penultimate chapter, work covering the central theme of this thesis; the investigation of block copolymers as templates for the cross-phase alignment of segmented nanorods, is presented. The main objective of this work is to perform an initial proof of principle experiment under optimised conditions to determine if successful cross-phase alignment of nanoparticles (i.e. interactions between block copolymer and segmented nanorods resulting in alignment of the nanorods across the block copolymer microphases) may be achieved within block copolymers. If successful, further experiments will then be performed to explore the effect of different parameters upon this potential method of nanoparticle alignment. Before proceeding with these experiments however, it is important to first consider a number of factors that will dictate the experimental conditions that are to be used.

Optimised Conditions for Cross-Phase Alignment

For the most part, the experimental conditions used in this chapter are drawn from those used in chapter 2 to form microphase separated block copolymer films, the difference being that segmented nanorods are dispersed in the polymer solution prior to microphase separation. As discussed in section 1.5 of chapter 1, the experimental conditions pertaining to the inclusion of the nanorods should be selected in order to maximise the enthalpic drive towards cross-phase alignment of the segmented nanorods, while minimising the entropic penalty for doing so, in order to maximise the probability of cross-phase templating. These conditions are as follows:

- Nanorod segment dimensions < microphase dimensions.
- Small nanorod concentrations
- Segment functionalisation that is highly selective towards the targeted microphases.

Satisfying the first condition listed above is perhaps the most critical, as it is viewed as the principle barrier to enabling cross-phase alignment of the nanorods (and consequently has been the focus of much of the work presented to this point in this thesis). Whilst it has been shown that such a combination of microphase separated block copolymers and segmented nanorods can be formed, it was discovered in the previous chapter that the conditions required to collect these nanorods also resulted in significant changes in the morphology of these nanorods: through breakage at the segment interfaces in addition to deformation (either plastically or by fragmentation) of the nanorod segments.

For the most part, these changes yield nanorods that are unsuitable for use in the proof of principle experiments. However, in the case of *aged* nanorod samples, a significant fraction of the nanorods remain with connected (although often deformed) segments, meaning that experiments to probe the use of block copolymers for cross-phase templating may still be performed using such nanorods. The use of these nanorods has an important consequence; the nanorods are necessarily limited to those with longer nickel segments, as the fragmentation type deformation that occurs at the surface of these segments (discussed in chapter 4) leads to reductions in segment size, which results in almost complete loss of the nickel segments when the segment length is ≤ 40nm long.

Of the available aged nanorod samples, the shortest nanorods that remain largely intact after collection consist of segments that are ~60nm long. These segment dimensions are smaller than the microphases in the lamellar diblock copolymer, but are larger than those in the spherical phase diblock copolymer. Thus, in order to minimise the degree of polymer chain stretching (and hence minimise the

decrease in entropy) when using these nanorods in proof of principle experiments, the lamellar diblock copolymer was used.

The second condition, use of a small number of nanorods in the polymer, is relatively simple to implement, though if the concentration is too low, then observing statistically significant numbers of nanorods in the polymer will be more difficult. In determining the nanorod concentration to be used initially, the number of nanorods typically produced from a single membrane template is first considered. On average, there are approximately 5.75 pores per μm^2 of membrane area (as demonstrated in an example SEM image in fig 5.1).
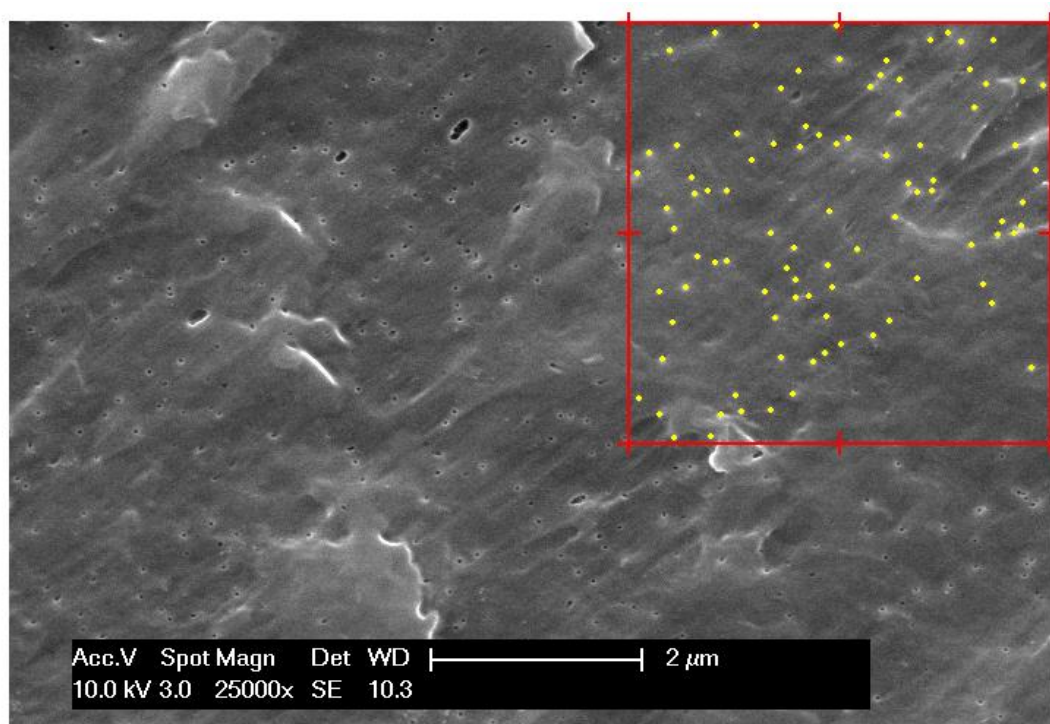
Fig 5.1: SEM image of the surface of a track etched polycarbonate membrane serving as a synthesis template for the segmented nanorods (pores are highlighted in yellow).

The total membrane surface area exposed to the metal plating solutions is dictated by the O-ring used in the experimental apparatus, which has a diameter of 3.4cm, Hence:

$$\text{Exposed membrane area} = \pi\,(1.7 \cdot 10^4)^2 = 9.0792 \cdot 10^8\,\mu m^2$$

Therefore, the total number of pores exposed to the plating solutions (and consequently the total number of nanorods formed per membrane) is:

$$9.0792 \cdot 10^8 \times 5.75 = 5.2205 \cdot 10^9\ \text{nanorods}$$

If this number of nanorods is added to a polymer solution prepared in the same manner as described in chapter 2, then the volume % of the polymer occupied by Au-Ni nanorods with segment dimensions of 60nm length and 40nm diameter (assuming an averaged polymer density of 1.075g/cm^3) is 0.0126%. This volume % (and significant fractions thereof) is deemed to be sufficiently low for the initial conditions of the proof of principle experiment, but not so low that nanorods will not be observed in sufficient numbers for analysis.

In order to fulfil the final condition, the nanorod segments will be selectively functionalised with short polymer chains of the same type as the targeted microphases at a high area chain density (number of polymer chains per unit surface area of the nanorods), as it has been shown in the literature that these conditions result in a strong enthalpic driving force for selective sequestration. [1, 2] Poly(styrene) (Mn: 1100 PDI: 1.11) and Poly(2-vinyl pyridine) (Mn: 2200 PDI: 1.16) polymer chains at area chain densities of at least 1.6 chains / nm^2 [3] are selected for this purpose. The selectivity of this functionalisation is ensured by using short polymer chains with terminal functionality; thiol groups on the P2VP chains to bind to the gold nanorod segments and carboxylic acid groups on the PS chains to bind to the nickel nanorod segments, as discussed in section 2.4.3 and 4.1.

Other Considerations

In addition to implementing these optimised conditions, there are a number of other considerations that also need to be taken into account. Foremost, the restriction to relatively large nanorods gives rise to the possibility that the nanorods could settle out by gravity in the polymer solution over the course of the microphase separation process, thereby affecting the distribution of nanorods and hence the cross-phase templating. In order for such settling to occur, the energy associated with gravitational settling of the nanoparticles must overcome the thermal energy that contributes to Brownian motion: [4]

- Energy of gravitational settling $= \Delta mgh$

where Δm = mass of nanoparticle less the mass of the solvent, g is acceleration due to gravity ($9.80665 ms^{-2}$) and h is the height of the swollen polymer film (the bulk of the solvent from the deposited solution evaporates rapidly).

- Thermal energy $= k_B T$

where k_B is the Boltzmann constant ($1.3806503 \cdot 10^{-23}$ $m^2 kg\ s^{-2} K^{-1}$) and T is the temperature (K).

And therefore;

$$k_B T \leq \Delta mgh$$

In the case of these nanorods, their mass is estimated from the dimensions of the nanorod segments before collection (as deformation results in the same or smaller nanorod masses):

Volume per segment $= \pi r^2 l = \pi (20 \cdot 10^{-7} cm)^2 \cdot (60 \cdot 10^{-7} cm) = 7.54 \cdot 10^{-17} cm^3/segment$

Gold segment mass $= 7.54 \cdot 10^{-17} cm^3 \cdot 19.3 g/cm^3 = 1.455 \cdot 10^{-15} g$

Nickel segment mass $= 7.54 \cdot 10^{-17} cm^3 \cdot 8.902 g/cm^3 = 6.712 \cdot 10^{-16} g$

Yielding a total nanorod mass of $2.126 \cdot 10^{-15} g$.

The mass of solvent (almost entirely dichloromethane) displaced by these nanorods is:

$7.54 \cdot 10^{-17} cm^3 \cdot 1.3255 g/cm^3 = 1.9989 \cdot 10^{-16} g$

Therefore, $\Delta m = 1.3255 \cdot 10^{-15} g - 1.9989 \cdot 10^{-16} g = 1.1256 \cdot 10^{-15} g$

So, given that room temperature conditions are used for the film formation process (T = 298K), $h \geq 3.727 \cdot 10^{-4}$ m in order for gravitational settling to influence the particle distribution. In this work, such settling appears to be unlikely given that the anticipated thickness of the *dry* films is on the order of 10 - 20 μm[*] (~20 fold smaller), meaning that the experimental conditions do not need to be modified to compensate. This of course assumes that the particles do not aggregate, but this is also unlikely given the surface functionalisation makes the particles highly soluble in dichloromethane.

---

[*] This estimate is based on the thickness of the polymer films formed in chapter 3, which are formed under the same conditions as will be used in the work presented in this chapter.

5.2. Experimental Methods and Materials

5.2.1. Nanorod Functionalisation

To ensure that a polymer chain density in excess of 1.6 chains / nm^2 is present on the surface of the nanorods, functional polymer is added to a suspension of the nanorods in dichloromethane in excess of that which is required to achieve a *close packed* monolayer.

The amount of functional polymer thus required is calculated from an estimated surface area of $8.80 \cdot 10^{-10}$ cm^2 per nanorod segment (based on nanorods with 60nm long segments before deformation[†]) and the surface area occupied by thiol groups on gold (0.214nm^2) [5] and carboxyl groups on nickel (0.197nm^2) [6], which yields a total of $4.465 \cdot 10^4$ and $4.110 \cdot 10^4$ polymer chains that are required to functionalise the nickel and gold segments respectively.

Given that the number of nanorods used in a typical experiment is equal to that formed in a single membrane template ($5.2205 \cdot 10^9$ nanorods), a total of $2.331 \cdot 10^{14}$ polymer chains ($3.872 \cdot 10^{-10}$ mol) are required for the nickel segments and $2.146 \cdot 10^{14}$ ($3.565 \cdot 10^{-10}$ mol) polymer chains are required for the gold segments. This is equivalent to $4.259 \cdot 10^{-7}$g and $7.842 \cdot 10^{-7}$g respectively.

Thus, based on these calculations, the nanorods are functionalized by suspending the nanorods synthesized from one membrane in 2ml of dichloromethane, and then adding 200μl of a solution of 1.9mg of PS-SH and 1.9mg of P2VP-COOH in 10ml of dichloromethane ($3.8 \cdot 10^{-2}$g of each polymer). The suspension is then shaken and left for 24 hours in the dark to ensure that functionalisation takes place (left in the dark as thiol groups can be photoreduced). The excess used

---

[†] Deformation does not appear to result in significant increases in surface area of the nanorods, the only exception being when nanorods break at the segment interface, which yields a 12.5% increase in surface area due to the newly exposed surface.

ensures that such functionalisation is complete, but is small enough that it will not swell the block copolymer appreciably (0.56 wt%).

5.2.2. Solution Preparation

Polymer solutions containing nanorods are prepared by adding 0.5ml of a nanorod suspension (one membrane template of nanorods in 2ml of fresh dichloromethane) to a vial containing 6.8mg of PS-b-P2VP. The solution is then briefly sonicated (no more than 30 seconds) to dissolve the polymer and disperse the nanorods.

5.2.3. Microphase Separation

Microphase separation is performed in the same manner as described in chapter 2 (section 2.2.4) for PS-b-P2VP.

5.2.4. Sample Characterisation

Sample characterisation is performed in the same manner as described in chapter 2 (section 2.2.5), except that thicker cross-sections (~150nm) are collected, in order to increase the probability that nanorods are present within the sections.

Note: the increased thickness will have the effect of reducing image resolution, and may complicate image analysis by the increased image detail resulting from the various depths being superimposed onto the final composite image.

5.3. <u>Results and Discussion</u>

5.3.1. <u>Proof of Principle Experiment</u>

Initially, TEM images of film cross-sections in regions where there are no nanorods were collected (fig 5.2), showing that the block copolymer film has undergone a well ordered microphase separation. A total film thickness of ~10µm is also measured, agreeing well with the previous approximation used in the assessment of gravitational settling. The film maintains a high degree of morphological ordering throughout consistent with the narrow polydispersities of both polymer blocks and its high molecular weight. The fact that such regions devoid of nanoparticles are present is a result of the low particle concentrations used in this proof of principle experiment.
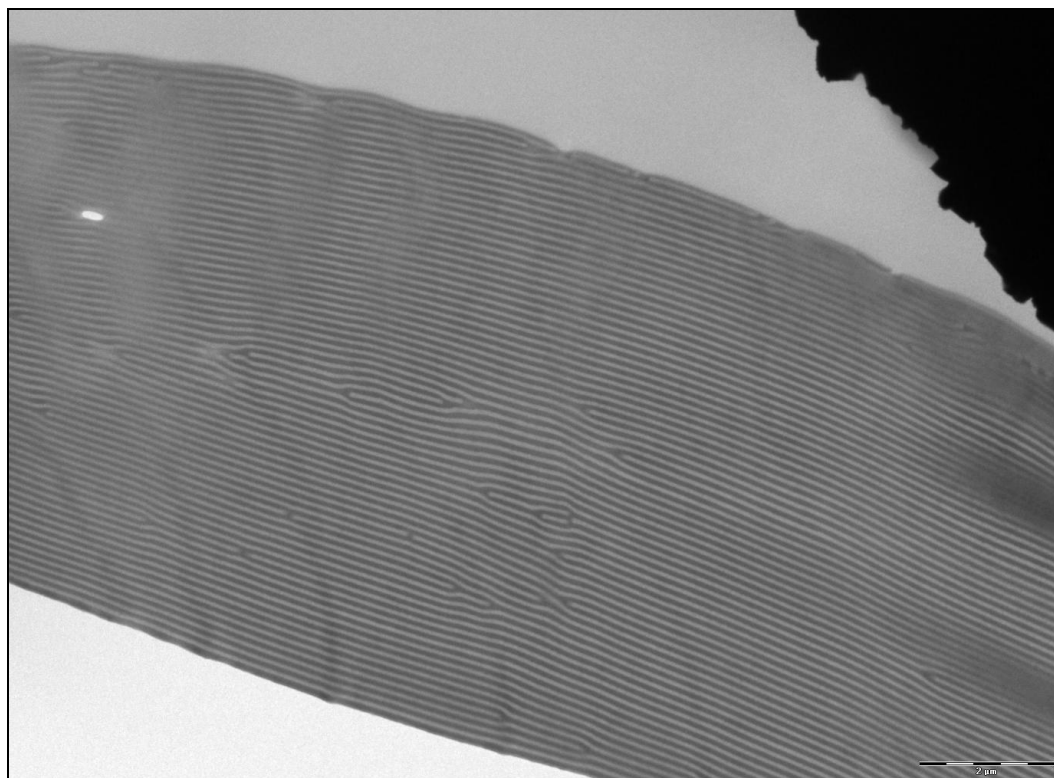
Fig 5.2: TEM image of a cross-section of the microphase separated block copolymer / nanorod films in regions absent of nanorods.

TEM images were then collected of regions of the polymer film where nanorods are present. Owing to the variety of nanoparticle sizes and compositions present in the film, a range of different (qualitative) observations were made.

First and foremost of these is the observation that intact bi-segmented nanorods (in cases where they are largely isolated from other nanorods) appear to be oriented perpendicular to the interface of the block copolymer microphases with the more electron dense (darker) gold segments existing within the compatible P2VP microphase and the less electron dense (lighter) nickel segments being located within the compatible PS microphase (fig 5.3 and 5.4), indicating that cross-phase alignment of segmented nanorods can occur under these optimized conditions. Notably, this appears to be the case for **all** such Au-Ni nanorods observed in the block copolymer film cross-sections.

The block copolymer surrounding the nanorods is also observed to retain its microphase separated structure, indicating that the entropic penalty associated with such templating (largely due to polymer chain stretching to accommodate the nanorods) is not significant enough to overcome the enthalpic drive towards microphase separation of the copolymer blocks. However, the entropic penalty for accommodation of these nanorods into the block copolymer microphases does appear to be sufficient to cause a small measure of disruption to the *ordering* of this microphase structure in the vicinity of such nanorods. This indicates that while some rotational/translational motion of the nanorods may be occurring to align with the microphases, the ordering of the block copolymer microphases is also being directed in part by the presence of the nanorods.
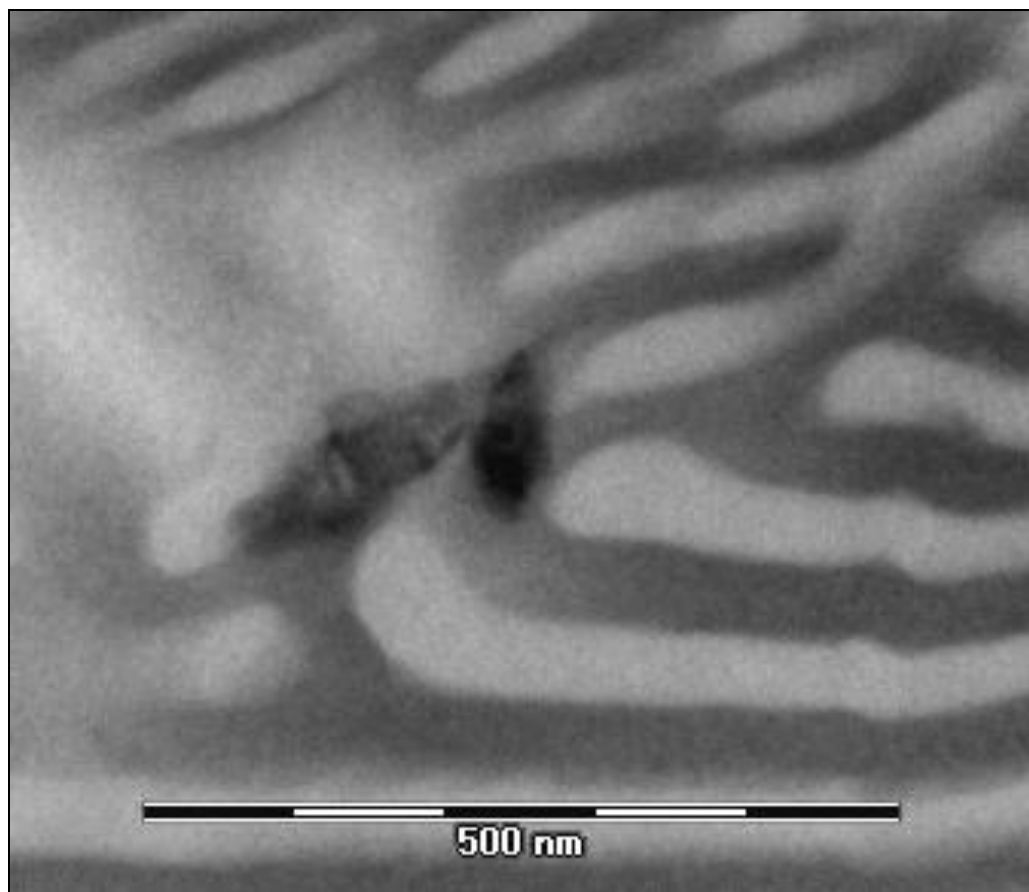
Fig 5.3: TEM image depicting cross-phase templating of segmented nanorods.
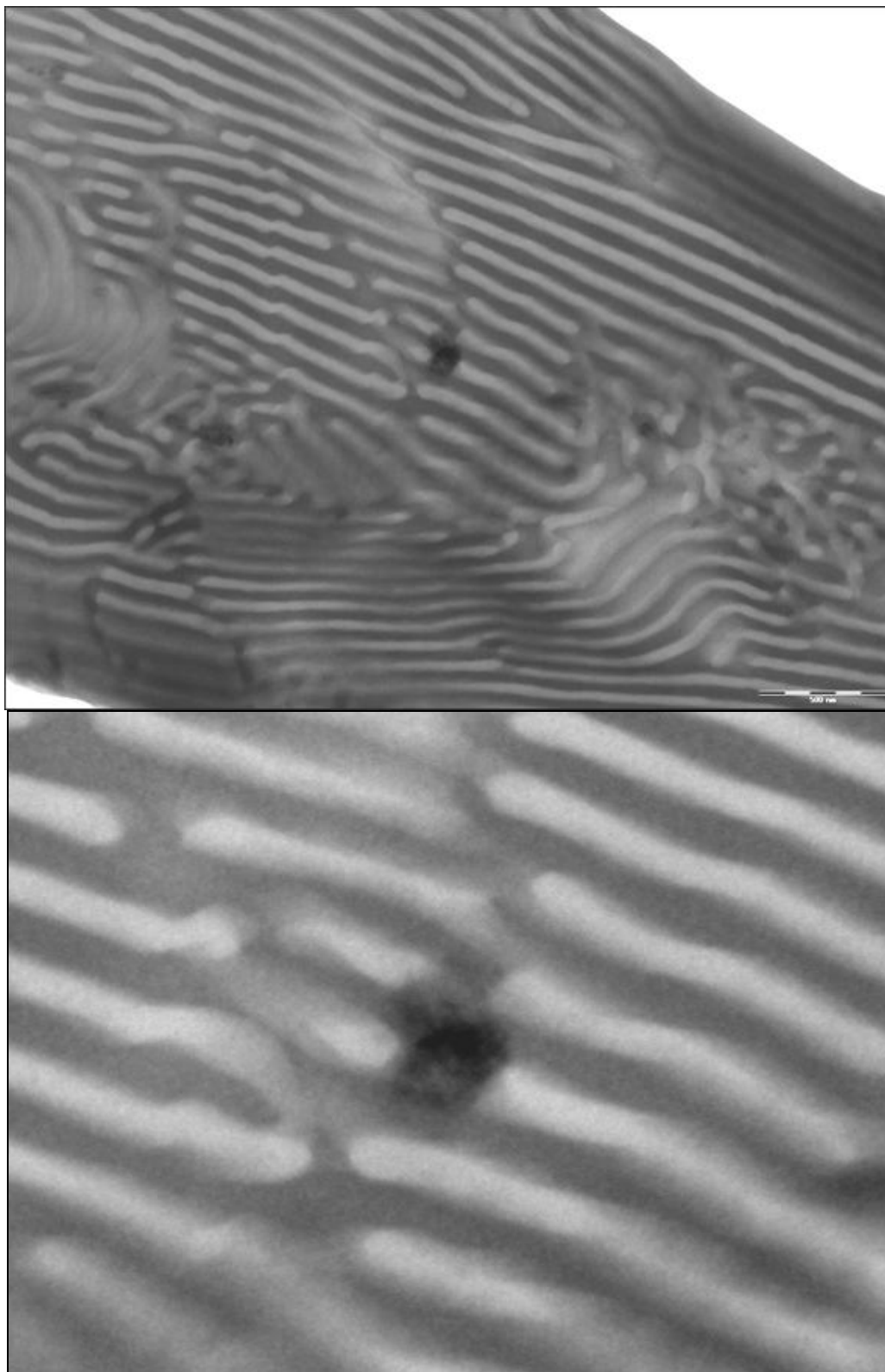
Fig 5.4: TEM image depicting cross-phase templating of segmented nanorods. Note that the apparent diameter of the nanorod in this image is larger than expected; likely as a result of two nanorods at different depths within the cross-section.

In the case of isolated single segment nanorods, the particles largely appear to be sequestered within single microphases (fig 5.5), although there appears to be some local distortion of the ordering of the block copolymer morphology to accommodate them. As with isolated, bisegmented nanorods, this was attributed to the entropic penalty associated with sequestration of the nanorods in a compatible microphase being significant enough to distort the microphases, but not so much that the microphase separation itself is disrupted. Note that while it is assumed that these single segment nanoparticles are located within a compatible microphase (based on results from the literature), this unfortunately cannot be verified in this case, as (1) there is connected metal segment with which electron density may be compared with and (2) EDAX only provides an overwhelming carbon signal from the surrounding polymer matrix.
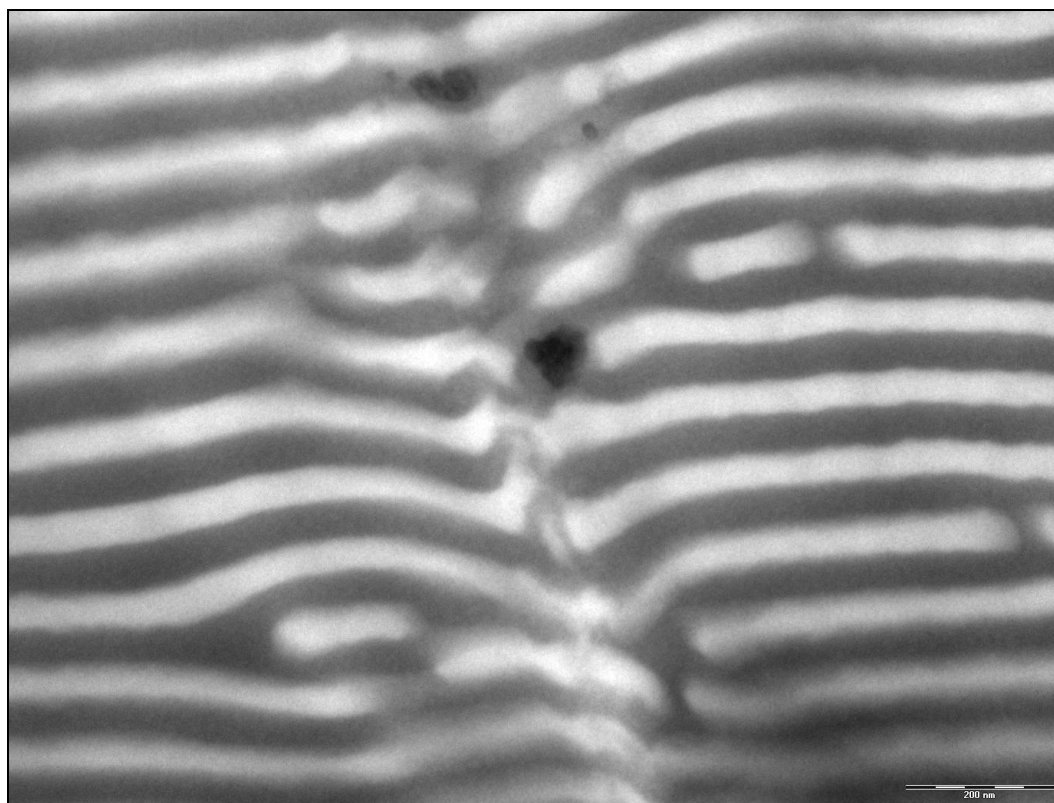
Fig 5.5: TEM image showing changes in microphase morphology to accommodate a single segment nanoparticle.

Notably, the above observations are not repeated when the nanoparticles are in close proximity to one another. In this case, there appears to be a local disruption in the microphase separation of the block copolymer film, which extends away from these particle clusters for ~100 – 200 nm. No discernable microphase separation and a seemingly random orientation of the nanoparticles occurs in this region (fig 5.6). This is most likely due to the significant degree of polymer chain stretching required to form ordered microphases adjacent to clusters of nanorods in close proximity, yielding an entropic penalty that is now significant enough to overcome the enthalpic drive towards microphase separation of the copolymer blocks. This result implies that high concentrations of nanoparticles within the polymer (with such large particle sizes) are undesirable.
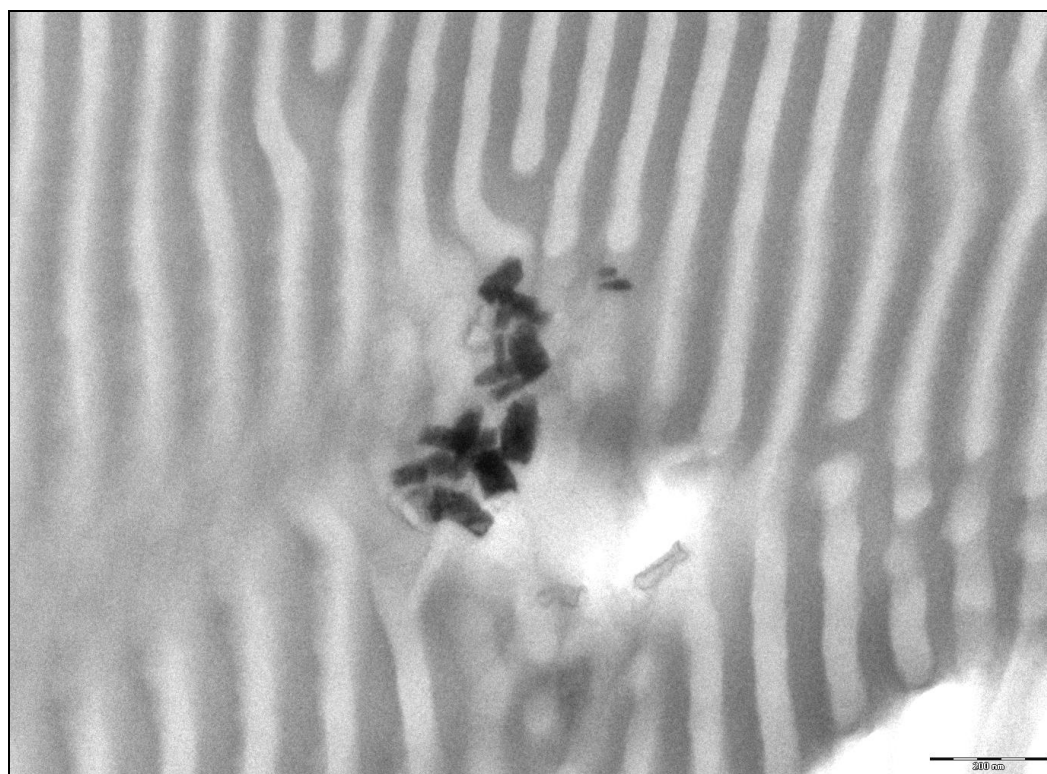
Fig 5.6: TEM image depicting changes in microphase morphology around nanorods in close proximity.

5.3.2. Influence of Experimental Conditions

From the results of the proof of principle experiment, it appears that cross-phase alignment of bisegmented nanorods can be made to occur under conditions that have been optimised for such behaviour. However, the ability to be able to use this method under less optimal conditions should be examined. It is important to investigate the effect of different parameters upon the cross-phase alignment of these nanoparticles, so that a clearer picture of how far these constraints may be relaxed while allowing cross-phase alignment emerges.

At this point, it should be mentioned that the range of parameters that may be tested in this work are more limited in scope than was originally intended i.e. no weakly segregated block copolymers. Nonetheless, there are several important experimental conditions that may be examined.

Selective Functionalisation

One such parameter is the selective functionalisation of the nanorods: is this required for cross-phase templating, or can an alternative, weaker enthalpic driving force be utilised? One way by which this may be tested in this system is to incorporate non-functionalised Au-Ni nanorods into the block copolymer, the enthalpic driving force being provided by the preferential segregation of the gold segments within the P2VP microphases of the block copolymer. [3] This by itself may not be sufficient for *cross-phase* alignment, as there is no enthalpic driving force directing the nickel segments towards selective segregation in the PS domains. However, as suggested by the results of the proof of principle experiment, cross-phase alignment appears to have a smaller degree of associated polymer chain stretching than incorporation of such large nanoparticles within a single lamellar microphase. On this basis, cross-phase alignment will be the preferable arrangement. A further concern in this experiment is the fact that the bare nanorods may aggregate as a result of their high surface energy. However, based on the literature, the interaction of the gold segments with the P2VP blocks

is anticipated to be sufficient to stabilise the nanorods in the polymer solution against aggregation. [7]

TEM images of non-functionalised Au-Ni nanorods in the block copolymer (formed under otherwise identical conditions to those used in the proof of principle experiment) are shown in fig 5.7 and 5.8. As indicated in fig 5.7, cross-phase alignment of the nanorods can occur in the absence of surface functionalisation, with virtually no disruption to the local microphase separation of the block copolymer. As with the functionalised Au-Ni nanorods, this is the case for all observed Au-Ni nanorods in the film cross-sections.

This result suggests that comparitively weak enthalpic driving forces for cross-phase templating may be used for cross-phase alignment, most likely because the entropic penalty for this arrangement is smaller compared to incorporation of both nanorod segments within a single microphase, but not so large that microphase separation is disrupted. As shown in fig 5.8 however, nanorods in close proximity result in disruption to the local microphase separation, similar to the results obtained when using functionalised nanorods.
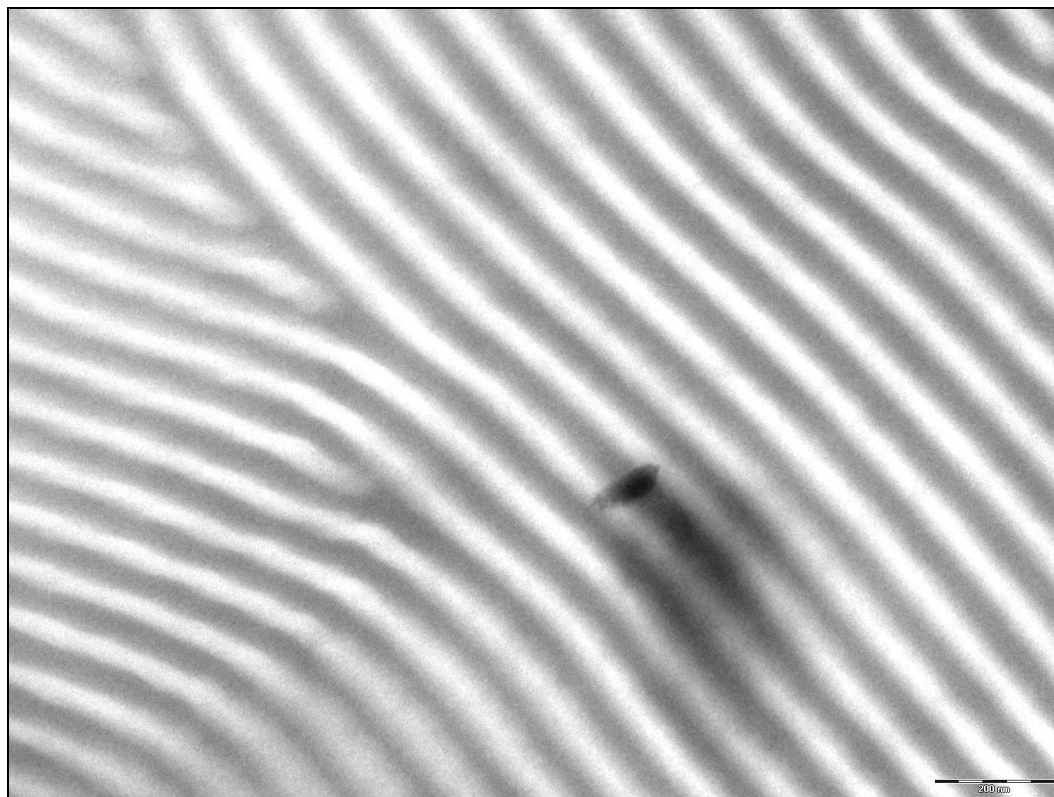
Fig 5.7: TEM image showing cross-phase templating of Au-Ni nanorods in PS-b-P2VP without surface functionalisation.
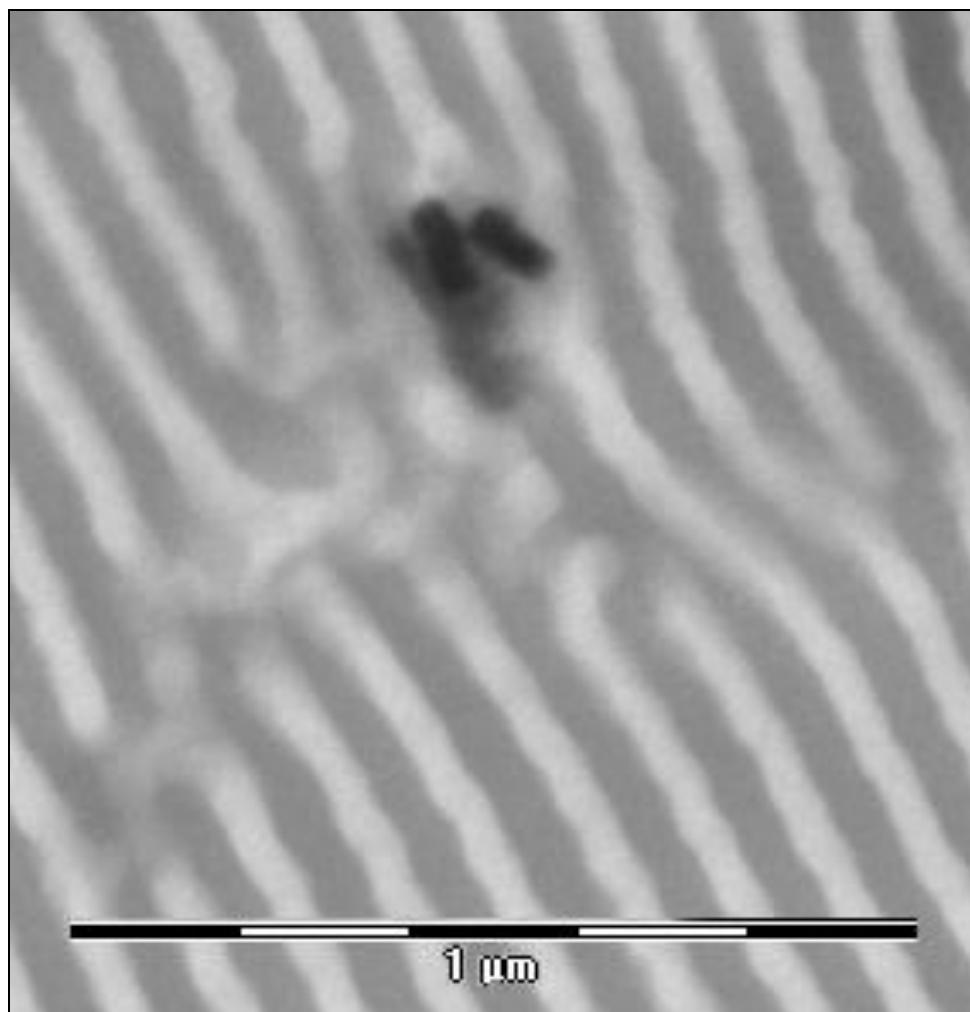
Fig 5.8: TEM image showing disruption of the local microphase separation in the presence of non-functionalised nanorods.

Nanorod Dimensions

Another important aspect of the system to investigate is the effect of the use of nanorods with segment lengths greater than the thickness of the sequestering microphases. To test this, nanorods with segment lengths ~15nm longer than the nominal lamellae thickness (prior to deformation) are incorporated into the block copolymers. TEM images of the resulting films (fig 5.9 and 5.10) suggest that these nanorods do not undergo cross-phase templating, instead resulting in severe disruptions to the local microphase ordering that extend some distance from the

isolated nanoparticles (up to ~500nm) before order is re-established. This may result from the excessive chain stretching required to accommodate such large nanoparticles combined with the selective functionalisation, which makes sequestration of the nanorods in the centre of the lamellar domains unfavourable (as occurs for large single segment nanorods). [8]
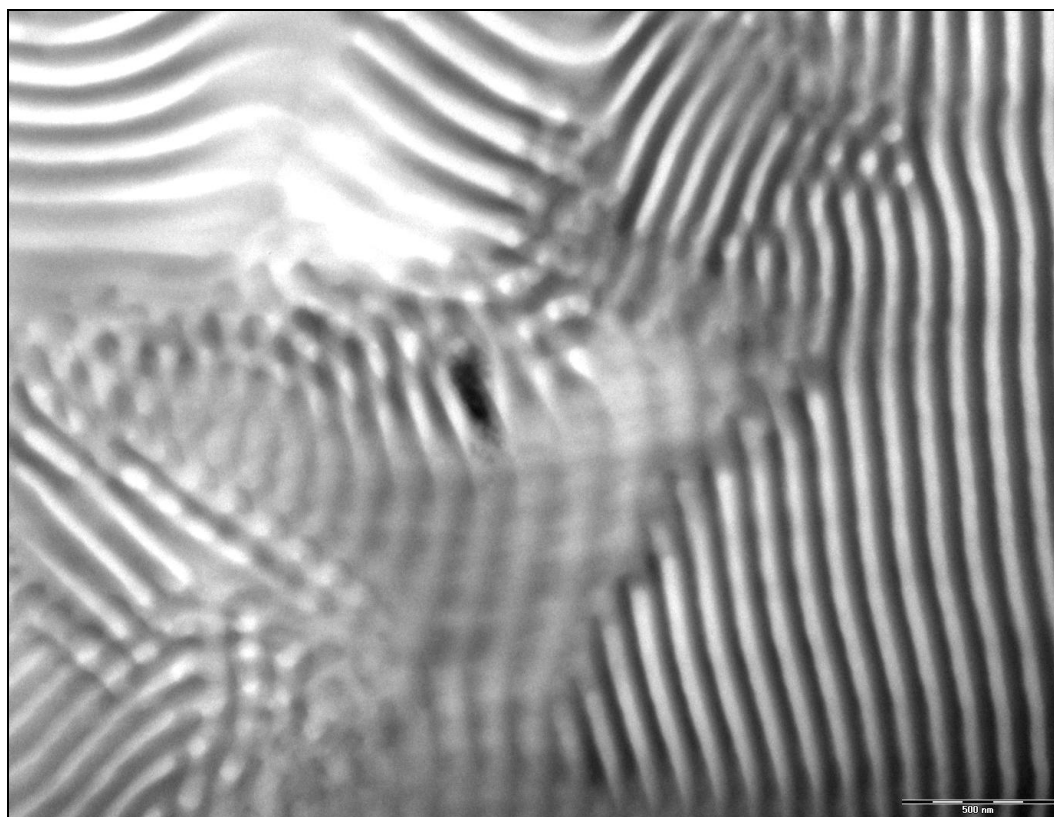
Fig 5.9: TEM image showing disruption of the local microphase ordering in the presence of long nanorods.
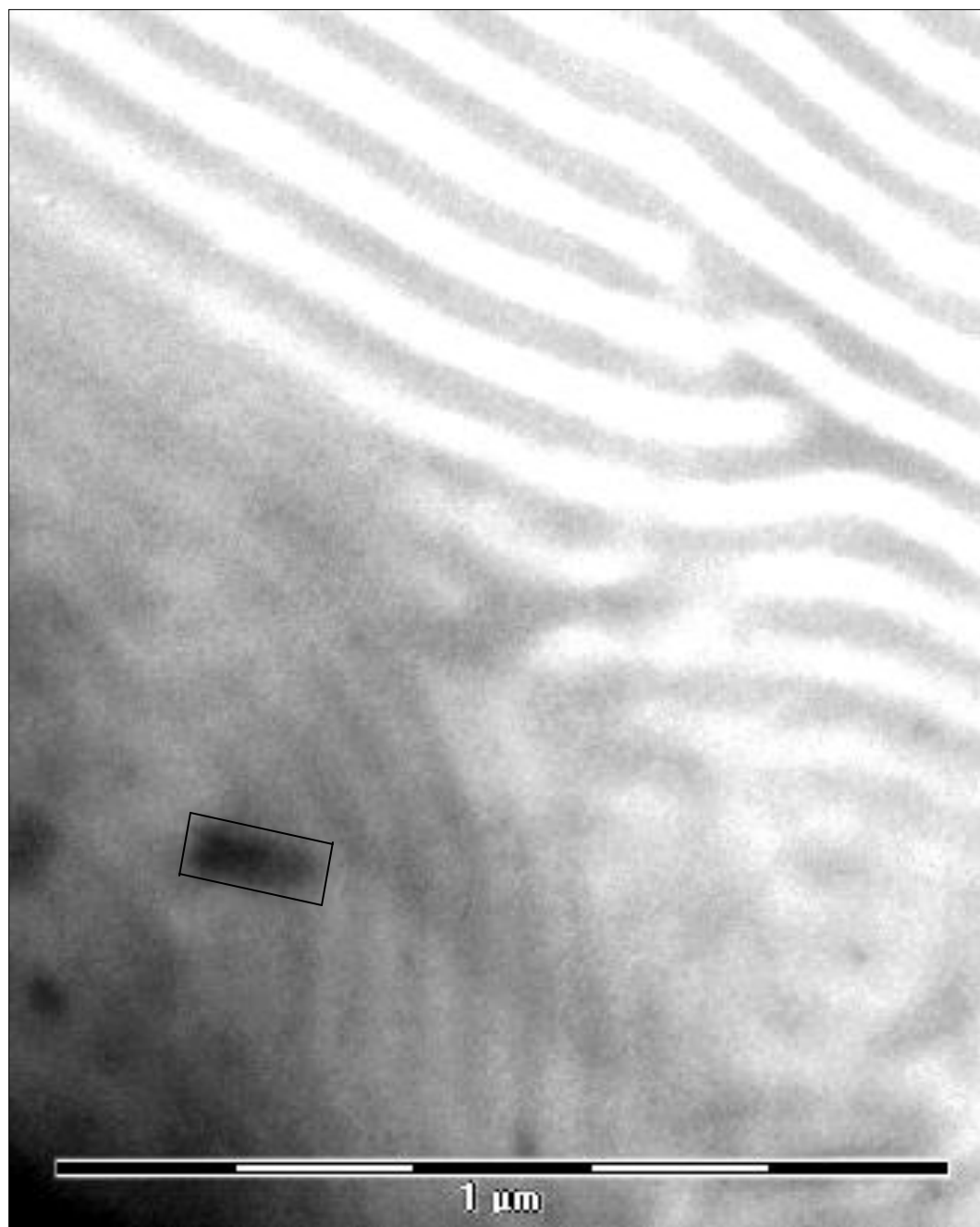
Fig 5.10: TEM image showing disruption of the local microphase ordering in the presence of long nanorods.

5.3.3. Influence of Morphology

An extension of the investigation into the effect of large (compared to the microphase dimensions) nanorods on cross-phase templating is to examine the effect of the smallest available nanorods on the spherical morphology PS-b-P2VP block copolymer, as this will yield an insight into how the different block copolymer morphologies change in response to the presence of particles that impart a high degree of polymer chain stretching.

As shown in figure 5.11, this film exhibits a high degree of order in regions where nanorods are absent. In the presence of nanorods (either single or bisegmented), the local microphase separation appears to be disrupted (fig 5.12), which is attributed to the high degree of chain stretching required to accommodate the nanoparticles. This is also observed for clusters of nanorods in close proximity (fig 5.13). Interestingly though, the disruption to the ordered sphere structure of the minority phase does not extend far into the film compared with the observations made for the lamellar diblock copolymer, microphase separation being re-established within 10-20nm of the isolated nanoparticles and ~50nm of the clustered nanorods.
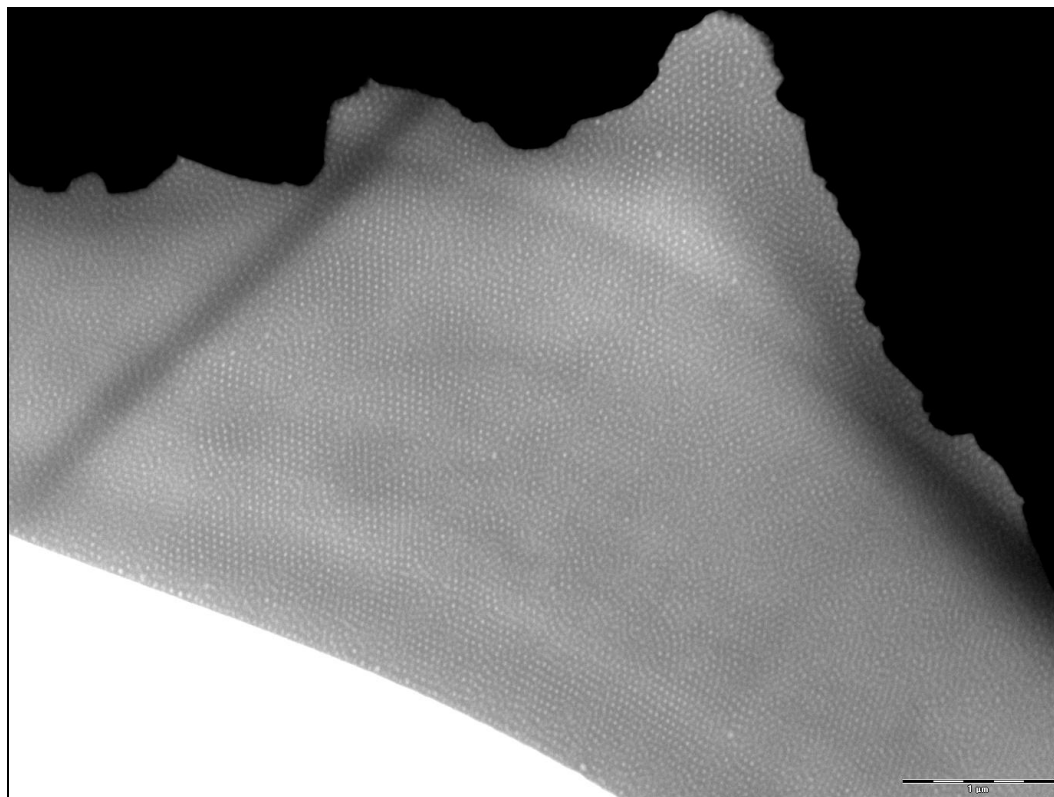
Fig 5.11: TEM image showing the BCC spherical morphology block copolymer in the absence of nanorods.
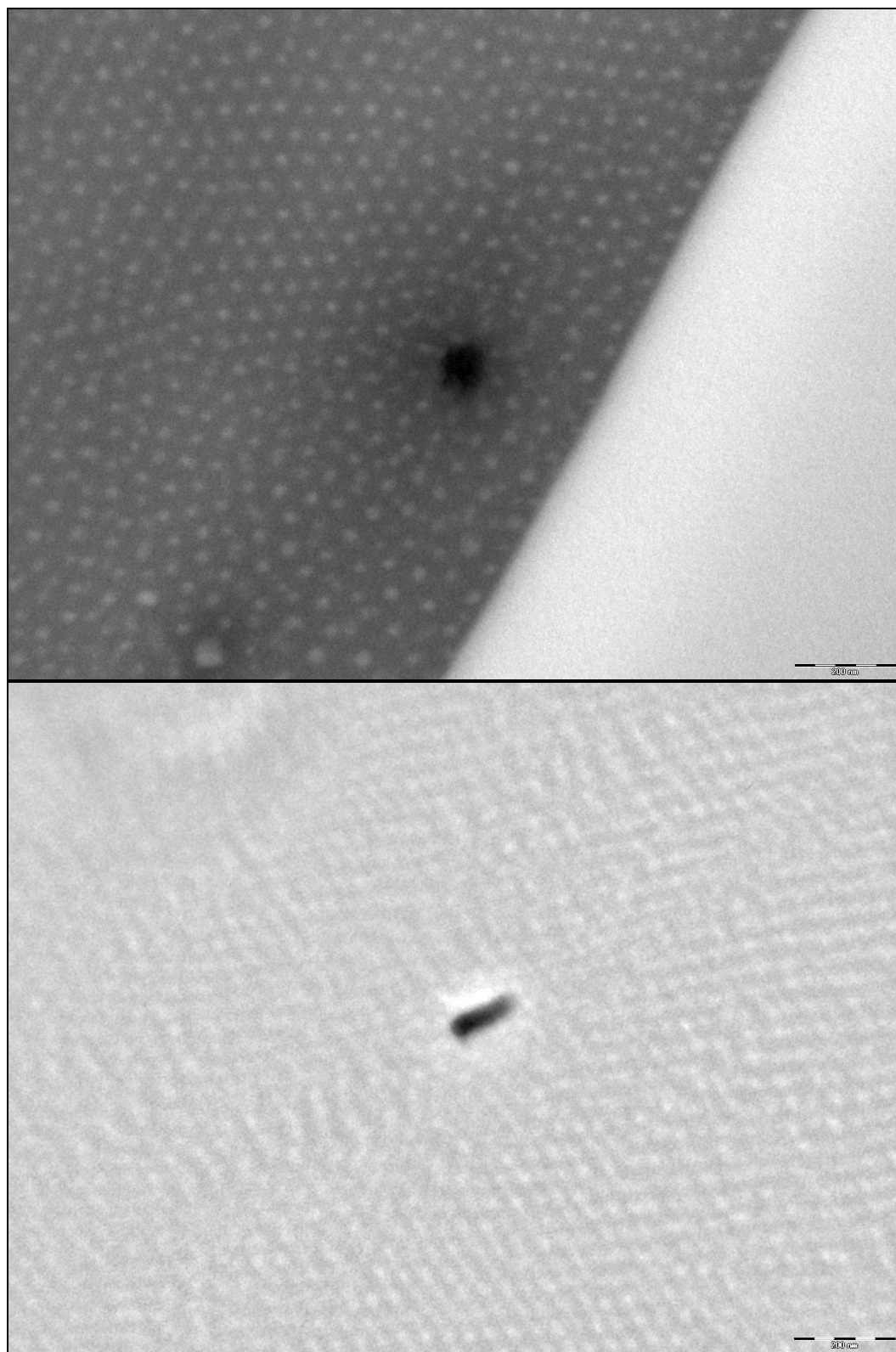
Fig 5.12: TEM image showing the effect of both single and bi-segmented nanorods on the microphase structure of PS-b-P2VP with a BCC spherical morphology.
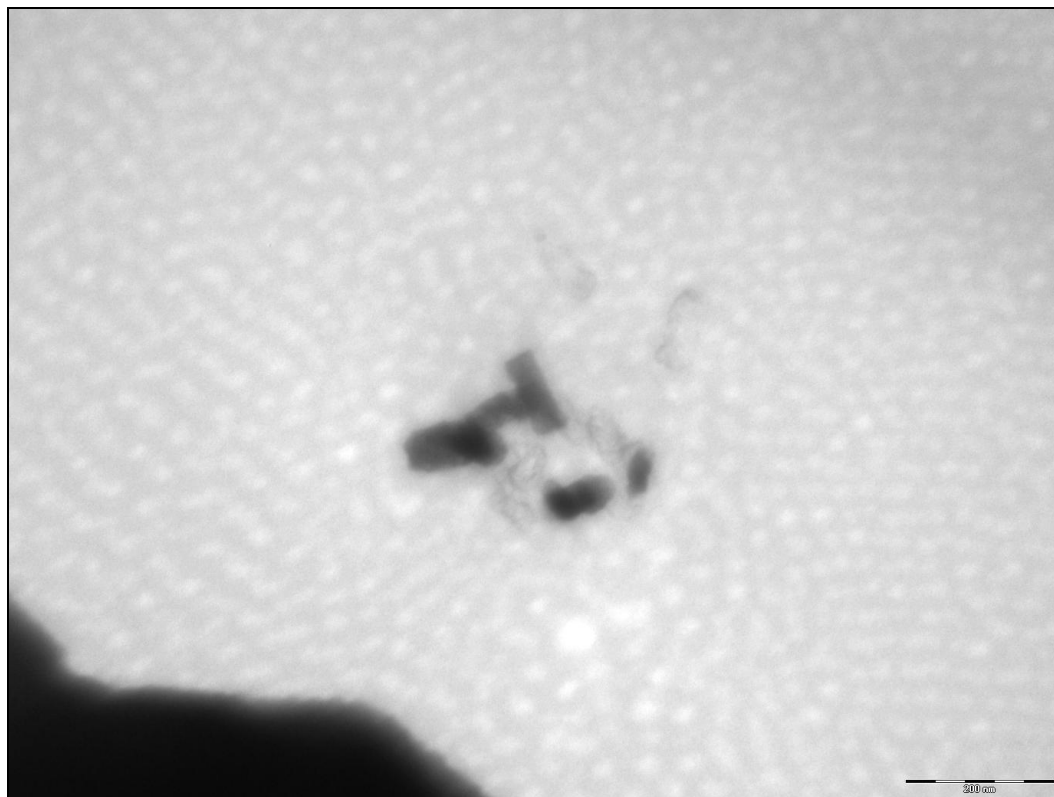
Fig 5.13: TEM image showing the effect of both a cluster of nanorods on the microphase structure of PS-b-P2VP with a BCC spherical morphology.

5.4. <u>Conclusions</u>

In conclusion, it was found in a proof of principle experiment that, in all observed instances, bi-segmented nanorods align across the phases of strongly segregated lamellar block copolymers under optimised conditions without any disruption to the local microphase separation of the block copolymer, although the ordering of the microphases was altered in the vicinity of the nanorods. This indicates that the entropic penalty associated with such alignment is not prohibitively high under these conditions. Single segment nanorods with dimensions that are an appreciable fraction of the microphase dimensions (resulting from deformations in the segmented nanorod samples during collection) appear to be sequestered within compatible microphases, but this is accompanied by changes to the local microphase morphology; a result that is attributed to a resolution between the enthalpic driving force towards inclusion in a compatible microphase and the polymer chain stretching i.e. entropic penalty associated with sequestration in an unperturbed microphase. This in turn implied that for these large particles, segregation within a single microphase is less entropically favourable than cross-phase templating.

Furthermore, it was found that these observations only applied to nanorods in isolation, as collections of nanorods in close proximity to one another resulted in disruption in the local microphase separation, regardless of the number of segments or segment composition. This latter effect was attributed to the entropic barrier, imposed by the chain stretching required being too high to accommodate these clusters of nanorods within a microphase structure.

Following this proof of principle experiment, further experiments were performed to investigate the robustness of this cross-phase templating process to a broader range of experimental conditions. In one such experiment, it was found that selective functionalisation of the nanorods is not required for cross-phase templating to occur; a weaker enthalpic driving force (only applied to a single nanorod segment) is sufficient, as cross-phase alignment of these large

nanoparticles appears to incur a smaller entropic penalty from polymer chain stretching compared to segregation within a single microphase. In another experiment, it was found that nanorods with segment lengths greater than the thickness of the lamellae microphases do not assemble across the microphase interface. Instead, there is a severe change in the order and morphology of the block copolymer micrphases in the region surrounding such nanorods. A similar result is also observed in the case of block copolymers with a spherical morphology, except here that the disorder due to the presence of the nanorods extends a smaller distance from the nanoparticle's surface.

Importantly, it should be noted that the observations made in this chapter are largely qualitative in nature, as the requisite low particle concentrations (and hence even smaller number of intact Au-Ni segmented nanorods), cross-section preparation method and reduced TEM resolution (and contrast) due to the presence of large amounts of electrically insulating (and stained) polymer make a quantitative analysis of the distribution of statistically significant numbers of particles in the block copolymers very difficult. Thus, despite the observations made in this chapter (in particular regarding cross-phase alignment) being the case for *all* such observed nanorods (thereby constituting evidence of the various nanoparticle's behaviours), it is acknowledged that quantitative data supporting these observations is necessary before it can be claimed with a high level of confidence that these observations are accurate.

5.5. <u>References</u>

1.   Chiu, J.J., Kim, B. J., Kramer, E. J., Pine, D. J., *Control of nanoparticle location in block copolymers.* Journal of the American Chemical Society, 2005. **127**: p. 5036.

2.   Chiu, J.J., Kim, B. J., Yi, G-R., Bang, J., Kramer, E. J., Pine, D. J., Macromolecules, 2007. **40**: p. 3361.

3.   Kim, B.J., Bang, J., Hawker, C. J., Kramer, E. J., Macromolecules, 2006. **39**: p. 4108.

4.   Van Der Zande, B.M.I., et al., *Colloidal dispersions of gold rods: synthesis and optical properties.* Langmuir, 2000. **16**: p. 451.

5.   Chabane Sari, S.M., et al., *Grafting colloidal stable gold nanoparticles with lissamine rhodamine B: an original procedure for counting the number of dye molecules attached to the particles.* . Journal of Materials Chemistry, 2004. **14**(3): p. 402.

6.   Ulmann, A., *An Introduction to ultrathin organic films: from Langmuir-Blodgett to self assembly.* 1991, San Diego: Academic Press.

7.   Van Der Zande, B.M.I., et al., *Aqueous gold sols of rod-shaped particles.* Journal of Physical Chemistry B, 1997. **101**: p. 852.

8.   Deshmukh, R.D., Liu, Y., Composto, R. J., Nano Letters, 2007. **7**(12): p. 3662.